PAPER Q

TOMOGRAPHY AND TOMOGRAPHIC MIGRATION USING RAY THEORY

Jerry M. Harris and Feng Yin

ABSTRACT

In this paper, we present wavefield tomography methods based on asymptotic ray theory. We introduce the concept of the wavefield tomography operator and compare it with traditional tomography methods. When the scattered fields, after being processed by a correlation procedure, are operated on with the tomography operator, we get an image of the velocity perturbation relative to a velocity background. If instead we input separated up-going and down-going reflection data into our tomography operator, we can get an image of reflectivity. With this general idea, we can develop and use tomographic reconstruction operators and algorithms not only for velocity inversion, but also for migration imaging. In the last part of this paper, we present simulation results and an example using real crosswell reflection field data. The results confirm that the algorithms are useful for crosswell imaging.

INTRODUCTION

Wave equation tomography is increasingly finding a place in crosswell data processing. Wave equation tomography methods, based on full wave theory, can be implemented in the time domain or in the frequency domain. In frequency domain, there is a very large matrix that occupies extremely large computer memory to be inverted (Harris and Yin, 1994). In the time domain, forward and back propagation computations cost too much CPU time (Tarantola, 1984) and also occupy significant computer memory. In addition, when the frequency is very high, we must sample the imaging region into many pixels or nodes and calculate the fields and Green's functions at this fine scale. To avoid these problems, wave equation inversion methods using asymptotic ray theory have been introduced (Beylkin, 1985, Miller, et. al., 1987, Yin, 1993).

The methods described herein are based on the full wave theory. We use a L_2 norm objective function derived for multiple frequencies for the observed wavefield minus the calculated wavefield. Then, we can use a Frechét derivative of this objective function to update the velocity relative to a background medium as in the paper by Harris and Yin (1994). Due to some disadvantages of full wave theory tomography as we mentioned above, we prefer to use asymptotic ray theory which is not only suitable for velocity inversion but also for migration imaging. With ray theory, the phase of the Green's function in the background medium can be calculated accurately and we do not need to compute the fields many pixel locations or nodes, e.g. as with moment methods and finite difference methods. This advantage is very important in field data applications.

By applying the geometrical optical approximation and inverse Fourier transform to the Frechét derivative of our L_2 norm objective function, we obtain the Frechét derivative represented by wavefield data in time domain and use this function for velocity inversion. In order to understand the physical meaning of this function for inversion, we compare the result with traditional traveltime tomography. We find that the Frechét derivative corresponds to simple backprojection tomography (BPT) as it is applied to traveltime data (Herman, 1980). In traveltime BPT, traveltime data are backprojected into the image region along raypaths, but in this case, the scattering data are backprojected into the image region along isochronic lines. We call this procedure the tomographic operator, and accordingly the Frechét derivative is the local linearized BPT tomographic wavefield operator. In this way, we can develop many wavefield tomography operators for inversion. In this paper, we consider only the SIRT operator.

In addition, from the Fréchét derivative, we can see that a correlation process on the wavefield data is required. This is one of the main characteristics in these methods. If we omit this correlation term, we must separate up-going and down-going wave before the tomographic operator is applied to the wavefield. Otherwise, the image will be contain many artifacts because of mispositioning of waveforms at the boundaries of heterogeneities.

We find that if we input the scattering field data into our tomography operators, we can get velocity perturbation image; therefore, we call this procedure *wavefield tomography.* If we input the separated up-going and down-going reflection data, or reflection data after being processed by a correlation procedure, we obtain as image which is similar to that obtained from migration; therefore, we call this image *tomographic migration.* We applied our algorithms to synthetic data and field crosswell data. The results show that these methods are extremely useful.

WAVEFIELD TOMOGRAPHY AND TOMOGRAPHIC MIGRATION

The goal of the non-linear wave equation tomography is to minimize the L_2 norm objective function:

$$J(m)=\frac{1}{2}\sum_{\omega}^{\Omega}\sum_{g}^{G}\sum_{s}^{S}\|u^{o}(r_g,r_s,\omega)-u^{c}(r_g,r_s,\omega)\|_2 \qquad (1)$$

where u^O and u^C are the observed and calculated wavefield in frequency domain, ω and s and g denote the frequency and source and receiver locations, and

$$u^{o}(\mathbf{r},\omega)-u^{c}(\mathbf{r},\omega)=-\omega^2 S(\omega)\int_V \tilde{u}^{c}(\mathbf{r}',\omega)m(\mathbf{r}')G(\mathbf{r}_g,\mathbf{r}',\omega)d\mathbf{r}', \qquad (2)$$

where $m(\mathbf{r})=\dfrac{\delta c_0(\mathbf{r})}{c_0^3(\mathbf{r})}$, $c_0(\mathbf{r})$ is the velocity in the background media. The wavefield in this background medium is $u^c(\mathbf{r})=S(\omega)\,\tilde{u}^c$, where $S(\omega)$ is the spectrum of the source function. The Frechét derivative can be derived as

$$\frac{\partial J}{\partial m}=-\sum_{\omega,s,g}\omega^2[S(\omega)\tilde{u}^{c}(\mathbf{r},\mathbf{r}_s)G(\mathbf{r},\mathbf{r}_g)]^{+}\delta u(\mathbf{r}_s,\mathbf{r}_g,\omega) \qquad (3)$$

where $\delta u = u^o - u^c$, + denotes conjugate. Then, we can use above derivative to update the background model as following

$$c^{(q+1)}=c^{(q)}+\alpha\frac{\partial J}{\partial m}. \qquad (4)$$

We have implemented the above method as in the paper (Harris and Yin, 1994). However, the total field $\tilde{u}^c(\mathbf{r},\mathbf{r}_s,\omega)$ must be evaluated for each frequency. Because our method is derived in the frequency domain, it is non-local in space and thus requires much computer time and memory to implement. To avoid these computation problems, we applied geometrical optical and the Born approximation to implement our method in the time domain. In the time domain, the finite speed of propagation of waves is used to restrict the domain of influence at an image point.

Using geometrical optics, the Born approximation, and the inverse Fourier transform, the above expression for Frechét derivative can be written as

$$\frac{\partial J}{\partial m} = \sum_{s,g} \sum_{s,g} [a(\mathbf{r}_s, \mathbf{r}, \mathbf{r}_g)] \delta \bar{\bar{u}}(\mathbf{r}_s, \mathbf{r}_g, \tau(\mathbf{r}_s, \mathbf{r}, \mathbf{r}_g)) \quad (5)$$

where

$$\delta \bar{\bar{u}} = \dot{S}(-t) * \dot{S}(t) * \overline{\delta u}(\mathbf{r}_s, \mathbf{r}_g, \tau(\mathbf{r}_s, \mathbf{r}, \mathbf{r}_g)) \quad (6)$$

$$\delta \bar{u}(\mathbf{r}_s, \mathbf{r}_g, t) = \int_V m(\mathbf{r}') u^c(\mathbf{r}', \mathbf{r}_s, t) * G(\mathbf{r}_g, t | \mathbf{r}', 0) d\mathbf{r}' \quad (7)$$

where $a(\mathbf{r}_s, \mathbf{r}, \mathbf{r}_g) = A(\mathbf{r}, \mathbf{r}_s) A(\mathbf{r}, \mathbf{r}_g)$, $\tau(\mathbf{r}_s, \mathbf{r}, \mathbf{r}_g) = T(\mathbf{r}, \mathbf{r}_s) + T(\mathbf{r}, \mathbf{r}_g)$, and A and T satisfy the transport and eikonal equations, respectively. Using the geometrical optics approximation, we have

$$\overline{\delta u}(\mathbf{r}_s, \mathbf{r}_g, t) = \int_V m(\mathbf{r}') a(\mathbf{r}_g, \mathbf{r}', \mathbf{r}_s) \delta(t - \tau(\mathbf{r}_g, \mathbf{r}', \mathbf{r}_s) d\mathbf{r}' \quad (8)$$

From equations (5)-(6), we can see that a correlation procedure must be applied to the source function in wavefield tomography in order to obtain a zero phase time function $W(t)=\dot{S}(-t) * S(t)$; therefore, the convolution between W(t) and $\overline{\delta u}(\mathbf{r}_s, \mathbf{r}_g, t)$ does not change the phase of $\overline{\delta u}(\mathbf{r}_s, \mathbf{r}_g, t)$. and it is not necessary to separate the down-going wavefield from the up-going wavefield in wavefield tomography method. This separation step is usually required in cross-hole migration. In addition, although the forward calculation of the wavefield requires accurate computation of u^c and updating the model using equation (4) is done repeatedly, we can reach the goal of velocity inversion when the function J(m) tends to zero. We can also conduct one iteration inversion for imaging a velocity perturbation under the linear assumption, using equation (5).

After we compare equation (5) with simple traveltime backprojection tomography (BPT), we find that equation (5) is almost the same as traveltime BPT except for the weight. In traveltime BPT, we backproject the traveltime along the ray path. In wavefield imaging, we backproject the wavefield $\delta \bar{\bar{u}}(\mathbf{r}_s, \mathbf{r}_g, t)$ along isochronic lines with the specified weight. So we call the right hand side of equation (5) the BPT wavefield tomography operator. Whenever it acts on the wavefield $\delta \bar{\bar{u}}(\mathbf{r}_s, \mathbf{r}_g, t)$, we can get the velocity perturbation. The forward operator corresponding to this tomography operator is

$$\bar{\bar{\delta}} u(\mathbf{r_S}, \mathbf{r_g}, t) = \int_V \frac{\partial J}{\partial m} a(\mathbf{r_g}, \mathbf{r}', \mathbf{r_S}) \delta(t - \tau(\mathbf{r_g}, \mathbf{r}', \mathbf{r_S}) d\mathbf{r}' \quad (9)$$

In order to improve the image resolution, we can also modify the weight when we backproject the wavefield $\delta\bar{\bar{u}}(\mathbf{r}_s,\mathbf{r}_g,t)$ along isochronic lines and develop other methods to invert for function $f(\mathbf{r})=\frac{\partial J}{\partial m}$. Next, we will develop SIRT wavefield tomography to invert for function $f(\mathbf{r})$ as follows.

Considering the k^{th} isochronic plane $I(t_k)$, the equation (9) can be discretized as

$$d_k = \sum_n c_{kn} \cdot f_n \tag{10}$$

where

$$c_{kn} = \sum_m a(l_{km}) \cdot \rho_{nkm} \cdot \Delta s \tag{12}$$

where d_k is the k^{th} sampling point of the wavefield $\delta\bar{\bar{u}}(\mathbf{r}_s,\mathbf{r}_g,t)$, $a(l_{km})$ is the value of the amplitude $a(\mathbf{r}_g,\mathbf{r}',\mathbf{r}_s)$ at the point l_{km}, ρ_{nkm} is the pulse basis function, Δs is the integral step. Then, we have the following SIRT iterative form for $f(\mathbf{r})$

$$f_n^{(q+1)} = f_n^{(q)} + \beta \sum_k \frac{c_{kn}}{\sum_n c_{kn}^2} (d_k - \sum_n c_{kn} \cdot f_n) / z_n \tag{13}$$

where, β is a damping factor, z_n is the non-zero numbers of c_{kn} $(1 \le k \le L \cdot S \cdot R)$. We call the above inversion method the SIRT wavefield tomography operator. To use this operator, we must know the isochronic lines in the background media for distribution of $f(\mathbf{r})$ along it.

The BPT and SIRT wavefield tomography operators for velocity perturbation are obtained next. By comparing the inverse Radon transform(IRT) method(Miller, 1987) with traditional traveltime tomography, we know that the method corresponds to the convolution filtered backprojection tomography method for traveltimes. For wavefield data, this would become IRT tomography wavefield operator. When we input the scattering data into each tomography operator, we can output the velocity perturbation related to the current background. All of the above methods are fast and accurate inversions.

But as we know, sometime, we are not only interested in velocity inversion, but also in geometry in the imaging region. Next we will extend our tomography operators to invert for geometry in the imaging region.

If we omit the correlation procedure in above inversion equations, and directly input the raw reflection data into our BPT wavefield tomography operator, we have

$$\frac{\partial J}{\partial m} = \sum_{s,g} [a(\mathbf{r}_s, \mathbf{r}, \mathbf{r}_g)] ref(\mathbf{r}_s, \mathbf{r}_g, \tau(\mathbf{r}_s, \mathbf{r}, \mathbf{r}_g)]. \tag{14}$$

Also, if we don't separate down-going and up-going wave and use equation (14) to backproject the reflection data into model space directly, we will obtain many artifacts for the reflectivity of a given layer. This is because reflections from opposite directions take opposite signs when viewed from above or below the layer (Hu, 1988). If we modify equation (14) as follow

$$\frac{\partial J^{up}}{\partial m} = \sum_{s,g} a(\mathbf{r}_s, \mathbf{r}, \mathbf{r}_g) ref^{up}(\mathbf{r}_s, \mathbf{r}_g, \tau(\mathbf{r}_s, \mathbf{r}, \mathbf{r}_g)) \tag{15}$$

$$\frac{\partial J^{down}}{\partial m} = \sum_{s,g} a(\mathbf{r}_s, \mathbf{r}, \mathbf{r}_g) ref^{down}(\mathbf{r}_s, \mathbf{r}_g, \tau(\mathbf{r}_s, \mathbf{r}, \mathbf{r}_g)) \tag{16}$$

then, we can get the migration image which represents reflectivity. This means if we input up-going or down-going wavefield into our wavefield tomography operator, we can get a migration image so we call the procedure tomographic migration. The operators are first developed for velocity inversion, but we apply them to reflection data to get the geometry image. We use Fig. 1 to show how the wave tomography operators for velocity inversion compare with migration imaging.

SYNTHETIC AND REAL DATA TESTS

A synthetic model for crosswell imaging is presented in Fig. 2. We placed 40 sources in the left hole and 40 receivers in the right hole. We then use a ray method to produce the scattering field data and use our BPT operator to get the velocity perturbation picture as shown in Fig. 3. Next, we place three sources on the surface and locate 40 receivers in left hole and 40 receivers in the right hole. If we don't correlate the scattering data, using the time function $\dot{S}(-t)$, and use our BPT and SIRT operators, we get the results shown in Fig. 4 and Fig. 5, respectively. These represent geometry images of the scattering region. From Fig. 5, we can see if we also put sources on the bottom and don't correlate with the time function $\dot{S}(-t)$, and input the scattering field excited by both the top and bottom sources, we will get a null picture, i.e., the top and bottom data will cancel.

CONCLUSIONS

In order to obtain a high resolution inversion image and save computation time and computer memory, two wavefield tomography operators using asymptotic ray theory have been developed. Through demonstration with a synthetic example and the field data example, we believe that our methods will become very useful tools not only for velocity inversion but also for migration imaging. Next we will apply our BPT and SIRT wavefield tomography operators to real scattering field data for velocity perturbation inversion.

ACKNOWLEDGMENTS

This work is supported by the Seismic Tomography Project of Stanford University, a research consortium sponsored by companies of the oil and gas industry. The second author would like to thank Nicholas Smalley for his help in obtaining the up-going and down-going wavefields for the Devine data set, and Youli Quan and Mark Van Schaack for their help in processing and plotting pictures with computer network of STP.

REFERENCES

Harris, J.M. and Feng Yin, Nonlinear-frequency wave equation inversion, in 1994 STP report

Herman, G.T., Imaging reconstruction from projections, Academic Press, New York,

Lazaratos, Spyros K., et. al., High resolution imaging with crosswell reflection data, Seismic tomography project, Vol. 2, No.1, 1991

Hu, L.Z, McMechan, G.A. and Harris, J.M., Acoustic prestack migration of cross-hole data, Geophysics, 53, 1015-1023, 1988

Miller D., Oristaglio, M., and Beylkin, G., 1987, A new slant on seismic imaging: Migration and integral geometry: Geophysics, 52, 943-964.

Tarantola, A., The seismic reflection inversion problem. In: Inverse problems of Acoustic and Elastic Waves: Santosa, F., Pao, Y.H.., Symes, W. and Holland, Ch.(eds.), Society of Industrial and Applied Mathematics, Philadelphia, 1984.

Yin Feng, Geophysical diffraction tomography using waveform as projection, 63th Ann. Intern. SEG. Mtg.., Expanded Abstracts:57-59, 1993.

Yin F., B.L. Gu and Y. Wei, Ray tracing tomography for cross-hole exploration, Chinese Journal of Geophysics, Vol. 34, No. 4, 667-666, 1991.

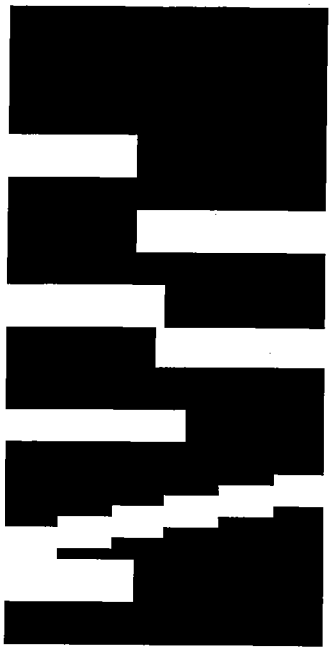

Figure 2:A scattering model for computer simulation.

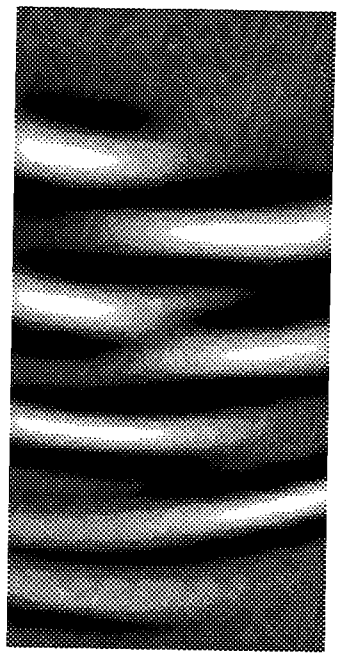

Figure 3: Velocity perturbation image by SIRT wave field tomography operator

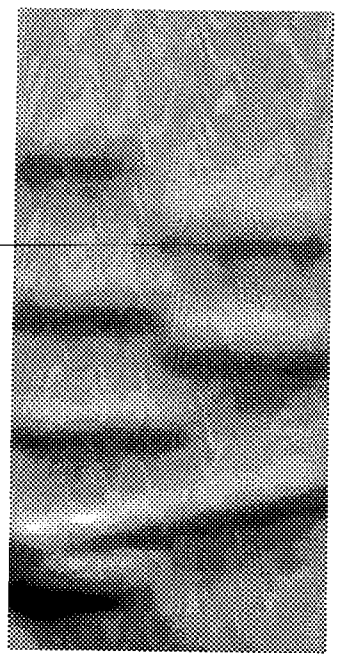

Figure 4: Geometry image of the scattering region by BPT wave field tomography operator

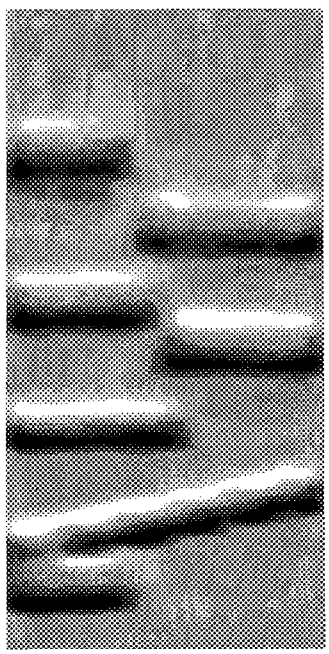

Figure 5: Geometry imaging of the scattering Region by SIRT wave field tomography operator

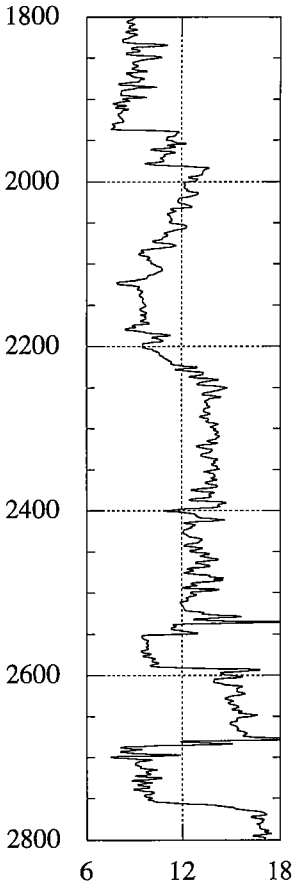

Figure. 6: Sonic log

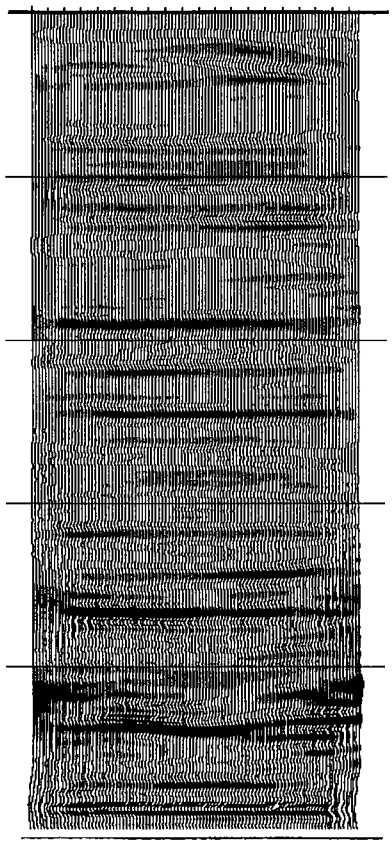

Figure 7: Reflection imaging by our BPT wave field tomography operator using Devine dataset

Figure 8: Traveltime tomography